Non-oxidative decomposition of methanol into hydrogen in a rotating gliding arc plasma reactor

Hao Zhang[a, b], Xiaodong Li[a,*], Fengsen Zhu[a], Zheng Bo[a], Kefa Cen[a], Xin Tu[b,*]

[a] State Key Laboratory of Clean Energy Utilization, Zhejiang University, 38# Zheda Road, Hangzhou, Zhejiang 310027, China

[b] Department of Electrical Engineering and Electronics, University of Liverpool, Brownlow Hill, Liverpool L69 3GJ, UK

ABSTRACT

A direct current rotating gliding arc (RGA) reactor co-driven by a magnetic field and tangential flow has been developed for the non-oxidative decomposition of methanol into hydrogen and other valuable products. The influence of input CH_3OH concentration and carrier gas (N_2 and Ar) on the reaction performance of the plasma process has been investigated in terms of the conversion of methanol, product selectivity, and energy efficiency of the process. The maximum CH_3OH conversion of 92.4% and hydrogen selectivity of 53.1% are achieved in the plasma methanol conversion using N_2 as a carrier gas. Optical emission diagnostics has shown the formation of a variety of reactive species (e.g., H, OH, CH, CN, N_2 and C_2) in the plasma decomposition of methanol. The vibrational and electronically excited species (e.g., $N_2\,(A^3\Sigma_u^+)$ and Ar*) could be critical in the conversion of CH_3OH, leading to a higher CH_3OH conversion in the CH_3OH/N_2 RGA due to the presence of more reaction pathways. Compared to other non-thermal plasmas, the RGA plasma shows a much better process performance, offering a promising and flexible route for hydrogen production.

Keywords: Rotating gliding arc; Methanol decomposition; Hydrogen production; Optical emission

* *Corresponding author.* Tel.: +86-571-87952037 (X. D. Li); +44-1517944513 (X. Tu)
E-mail address: lixd@zju.edu.cn (X. D. Li); xin.tu@liv.ac.uk (X. Tu)

spectroscopy; Reaction mechanisms

1. Introduction

Recently, the development of novel and cost-effective hydrogen production processes has attracted significant interest due to the depletion of fossil fuels and the environmental impact of the usage of fossil fuels. However, technical problems with the handling, storage, and transport of hydrogen largely limit its widespread use, particularly in portable fuel cells which have been considered as a promising alternative to the traditional battery technology [1]. The development of portable hydrogen generation systems could provide a source of clean hydrogen for portable fuel cells [2]. Methanol has been considered as an excellent H_2-containing source for portable hydrogen production due to its high hydrogen to carbon ratio, easy transportation, and low boiling point [3-8]. Catalytic steam reforming of methanol has been extensively investigated for hydrogen production [9]. However, this process still faces technical challenges that limit its use in a commercial-scale system. Although significant efforts have been devoted to find active, stable, and cost-effective catalysts for producing hydrogen from methanol, rapid deactivation of catalysts and the requirement of high temperature in the reforming process incur high energy and operational costs and consequently limit its industrial applications, particularly in on-board hydrogen production systems [10].

Non-thermal plasma technology provides an attractive alternative to the conventional catalytic route for methanol conversion at a relatively low temperature [1-8, 11, 12]. In non-thermal plasmas, the overall gas temperature can be as low as room temperature, while the electrons are highly energetic, with a typical electron temperature of 1-10 eV, which is sufficient to break down most chemical bonds of gas molecules and produce chemically reactive species including the excited atoms, ions and molecules for the initiation and propagation of chemical reactions [12]. High reaction rate and fast attainment of steady state in the plasma processes allows rapid start-up and shutdown of the plasma process, providing highly flexibility to be integrated into portable hydrogen production systems [11, 12]. Different non-thermal plasma systems have been developed for methanol conversion into hydrogen to maximize hydrogen production and energy efficiency of the plasma process, such as microhollow cathode discharge (MHCD) [2], microwave discharge [5-8], and dielectric barrier discharge (DBD) [13]. However, the relatively low power level of these plasma systems makes it difficult to achieve high, efficient conversion of methanol at a high gas flow rate, restricting the potential scale-up of this process [14]. For instance, Futamura et al. reported a methanol conversion of only 8-26% can be obtained at a feed N_2 flow rate of 100 ml/min and an input CH_3OH concentration of 1% in the plasma decomposition of methanol using a DBD [15].

Gliding arc discharge (GAD) has been considered as a transitional plasma with a relatively high electron density and high flexibility to work in a wide range of reactant flow rates and plasma power levels (up to several kW) [11, 16-18]. In a traditional GAD reactor that consists of two divergent knife-shaped electrodes, high flow rate (e.g., 10-20 l/min) is generally required to push the arc moving along the electrodes, generating a discharge zone for chemical reactions. As a consequence, the fast gas speed and limited two-dimensional plasma reaction area confined by the flat electrodes lead to a low retention time of reactants, thereby limiting the conversions of reactants and the energy efficiency of the plasma process [14, 19].

A direct current (DC) rotating gliding arc (RGA) co-driven by a magnetic field and tangential flow has been developed for hydrogen production from methane conversion in our previous work [19]. Compared to the traditional gliding arc system with knife-shaped electrodes, the RGA reactor can generate a synergetic effect resulting from the combination of swirling flow and Lorentz force, which can make the arc rotate rapidly and steadily without extinction (with a rotational speed of up to 100 rotations per second) with a wide range of gas flow rate (e.g., 0.05-40 l/min), creating a three-dimensional stable plasma area with the increased retention time of the reactants in plasma chemical reactions. Our previous study showed that this RGA system significantly improved the performance of plasma methane conversion with a maximum CH_4 conversion of 91.8%, a hydrogen selectivity of 80.7% and a maximum energy yield of H_2 of 22.6 g/kWh [19].

In this study, an RGA plasma reactor has been developed for the non-oxidative decomposition of methanol into hydrogen. N_2 and Ar have been commonly used as the carrier gases in the plasma processes for energy conversion and fuel production [2, 5, 20]. Significant efforts have been devoted to investigating the effect of different operating parameters (e.g., input power, flow rate, etc.) on the performance of plasma chemical reactions, whereas less attention has been paid to understand the role of different carrier gases in the plasma chemical processes. This is of primary importance because different carrier gases will generate different reactive species and significantly affect the plasma chemical reactions in different ways, especially the methanol decomposition process [19, 21]. In this work, the effect of input CH_3OH concentration and carrier gas (N_2 and Ar) on the reaction performance (e.g., conversion of methanol, selectivity of gas products, and energy efficiency) of the methanol conversion process has been investigated in an RGA plasma reactor. Optical emission spectroscopy (OES) has been used to give new insights into the formation of reactive species in the plasma chemical reactions. In addition, the possible reaction pathways in the plasma methanol decomposition process using different carrier gases have been discussed. Finally, a comparison of the methanol conversion process using different plasma systems has been carried out.

2. Experimental

2.1 Experimental setup and gas analysis

Fig. 1 shows the schematic diagram of the experimental set-up. A con-shaped stainless steel electrode (anode) is placed inside a circular stainless steel cylinder which acts as a cathode. A more detailed description of the RGA reactor can be found in our previous work [19]. The carrier gas (N_2 or Ar) was injected through three tangential inlets at the bottom of the reactor to form a swirling flow in the reactor. A magnet was placed outside the reactor to generate a magnetic field for the stabilization and acceleration of the arc. With the combined effect of swirling flow and Lorentz force, the arc moves upward and finally rotates rapidly around the inner electrode, forming a stable plasma volume for chemical reactions.

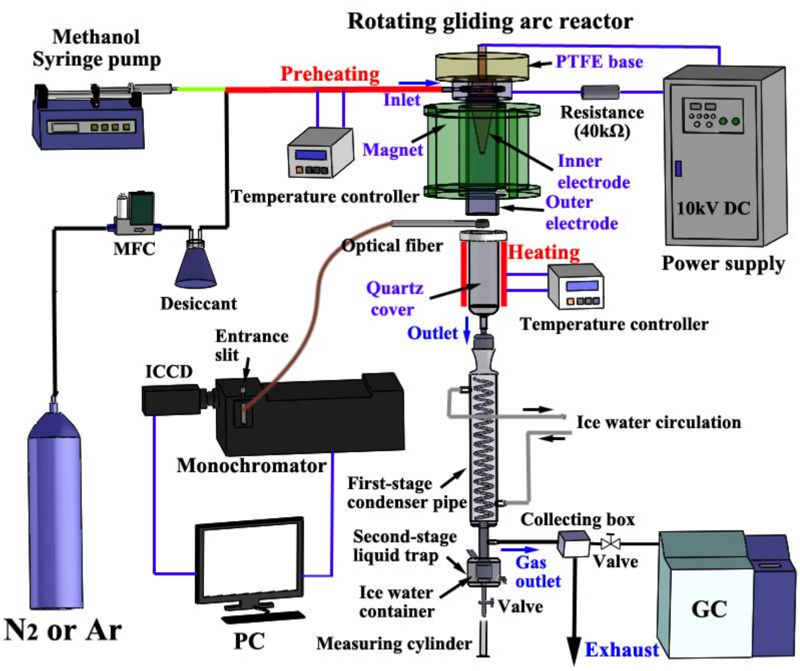

Fig. 1 – Schematic diagram of the experimental setup

Methanol was controlled and injected into the gas tube using a high-resolution syringe pump

(Harvard, 11 plus). In this way, the total feed flow rate (0.6 mol/min) of the mixed stream and input CH_3OH concentration (5-35 mol %) could be controlled. The mixed stream was then heated to 100 °C in a stainless steel pipe with an inner diameter of 4 mm (40 cm in length) equipped with a temperature controller system, to generate a steady-state vapor before flowing into the RGA reactor. The quartz cover of the plasma reactor was also heated to 100 °C to prevent any vapor condensation on the inner wall of the reactor. The plasma reactor was connected to a DC power supply (380 V/10 kV) with a 40-kΩ resistance connected in the circuit to limit and stabilize the breakdown current. A two-stage condenser was placed at the exit of the plasma reactor to collect the condensable vapors in the effluent: the first-stage condenser pipe was equipped with an ice water circulation system, while the second-stage liquid trap was placed inside the ice water container.

The gaseous products were measured by a gas chromatography (GC9790A, Fuli Analytical Instrument) equipped with a thermal conductivity detector (TCD) for the detection of H_2, O_2, and N_2 and a flame ionization detector (FID) for the analysis of CO, CO_2, and hydrocarbons. The condensed liquid was measured by a gas chromatography – mass spectrometry (JEOL, JMS-Q1050GC). We found the condensed liquid was mainly methanol with trace amounts of ethanol, propanol and ethylene glycol. Thus, the volume of the condensed liquid can be roughly regarded as the volume of the unreacted methanol after the plasma reaction [4, 6, 22-24]. The emission spectra of the plasmas were recorded by a 750-mm monochromator (PI-Acton 2750, grating: 1800 grooves/mm) equipped with an intensified charge-coupled device (ICCD, PI-MAX 2, 512×512 pixel). An optical fiber was placed at the exit of the RGA reactor to collect the plasma radiation.

2.2 Definition of parameters

For the plasma methanol decomposition process, the conversion of CH_3OH is defined as:

$$X(CH_3OH)(\%) = \frac{\text{moles of } CH_3OH \text{ converted}}{\text{moles of } CH_3OH \text{ input}} \times 100\% \quad (1)$$

The selectivities (S) of the products can be calculated:

$$S(H_2)(\%) = \frac{\text{moles of } H_2 \text{ produced}}{2 \times \text{moles of } CH_3OH \text{ converted}} \times 100\% \quad (2)$$

$$S(CO)(\%) = \frac{\text{moles of CO produced}}{\text{moles of } CH_3OH \text{ converted}} \times 100\% \quad (3)$$

$$S(CO_2)(\%) = \frac{\text{moles of } CO_2 \text{ produced}}{\text{moles of } CH_3OH \text{ converted}} \times 100\% \quad (4)$$

$$S(C_mH_n)(\%) = \frac{m \times \text{moles of } C_mH_n \text{ produced}}{\text{moles of } CH_3OH \text{ converted}} \times 100\% \quad (5)$$

The energy yield of H_2 is defined as:

$$EY(H_2)\,(\text{g/kWh}) = \frac{\text{grams of } H_2 \text{ produced per min.}}{power\,(\text{W}) \times 60/3600000} \times 100\% \quad (6)$$

The energy conversion efficiency (ECE) of the process is calculated based on the change of the lower heating values (LHV) of the fuels before and after the reaction.

$$ECE(\%) = \frac{\sum p_i \times LHV_i}{power\,(\text{W}) \times 60/1000 + \text{moles of } CH_3OH \text{ converted per min} \times LHV_{CH3OH}} \times 100\% \quad (7)$$

Where p_i refers to the moles of produced fuel i (i: H_2, CO, CH_4, C_2H_4, and C_2H_2) per minute. (LHV_{H2} = 241.6 kJ/mol, LHV_{CO} = 283.0 kJ/mol, LHV_{CH4} = 803.7 kJ/mol, LHV_{C2H4} = 1331.5 kJ/mol, LHV_{C2H2} = 1265.376 kJ/mol, LHV_{CH3OH} = 638.5 kJ/mol)

3. Results and discussion

3.1 Plasma decomposition of methanol

H_2 and CO were the major gaseous products in the non-oxidative decomposition of methanol using the RGA plasma, while trace amounts of CO_2, CH_4, C_2H_2, and C_2H_4 (total selectivity: 1.1-3.8%) were also formed. C_2H_6 was only detected with a selectivity of 0.5% in the conversion of 5% methanol using the argon RGA plasma. Note that C_2H_6 was identified as the main C_2 hydrocarbons in plasma processing of hydrocarbons using dielectric barrier discharges [25, 26]. However, previous work has also shown the shift of the distribution of C_2 hydrocarbon from C_2H_6 to C_2H_2 and C_2H_4 in the dry reforming of methane and carbon dioxide using an AC gliding arc plasma [11]. No C_3 or higher hydrocarbons gases were detected in this experiment. In the plasma partial oxidation or steam reforming of methanol, significant undesired gaseous byproducts were often generated with high selectivity, such as HCHO (45-60% selectivity) [27] and CO_2 (11.8-95% selectivity) [13, 24], the plasma non-oxidative methanol decomposition process using an RGA reactor could produce much cleaner gas products of which the syngas is the main one.

The effect of input CH_3OH concentration on the discharge power of the CH_3OH/N_2 and CH_3OH/Ar RGA plasmas is shown in Fig. 2. As we can see, the discharge power (149.8-349.4 W) of the CH_3OH/N_2 plasma is much higher than that of the CH_3OH/Ar plasma (105.2-271.6 W) at the same CH_3OH concentration. In both plasma chemical reactions, the discharge power initially increases with the increase of the input CH_3OH concentration to 20%, over which the discharge power is saturated when further increasing the CH_3OH concentration to 35%.

Fig. 3 shows the effect of input CH_3OH concentration on the conversion of CH_3OH. Increasing the CH_3OH concentration leads to a significant decrease of the CH_3OH conversion, even though the discharge power of the plasmas is initially increased with methanol concentration. The conversion of CH_3OH is higher in the CH_3OH/N_2 plasma than that in the CH_3OH/Ar RGA at the same methanol concentration, since the higher discharge power is generated in the CH_3OH/N_2 plasma with more reaction pathways due to the formation of a variety of excited species such as vibrational excited N_2 and electronically excited N_2.

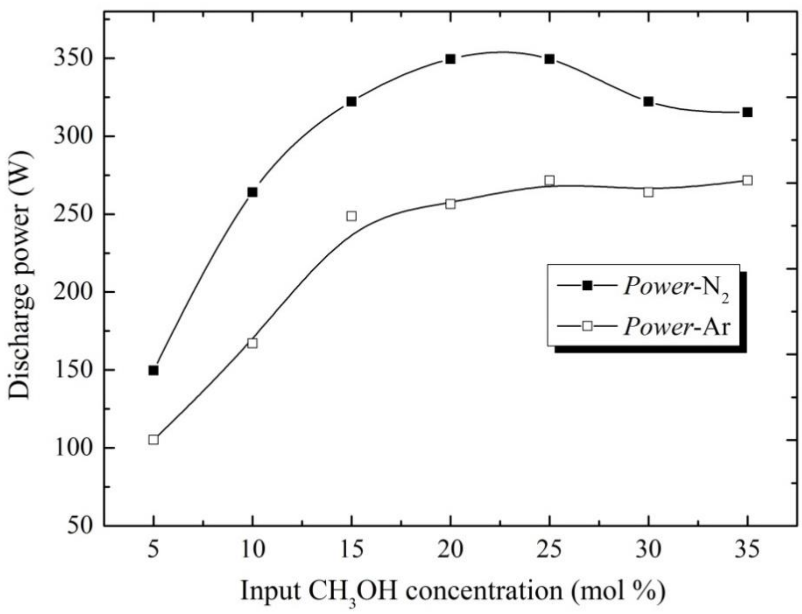

Fig. 2 – Effect of input CH_3OH concentration on the discharge power

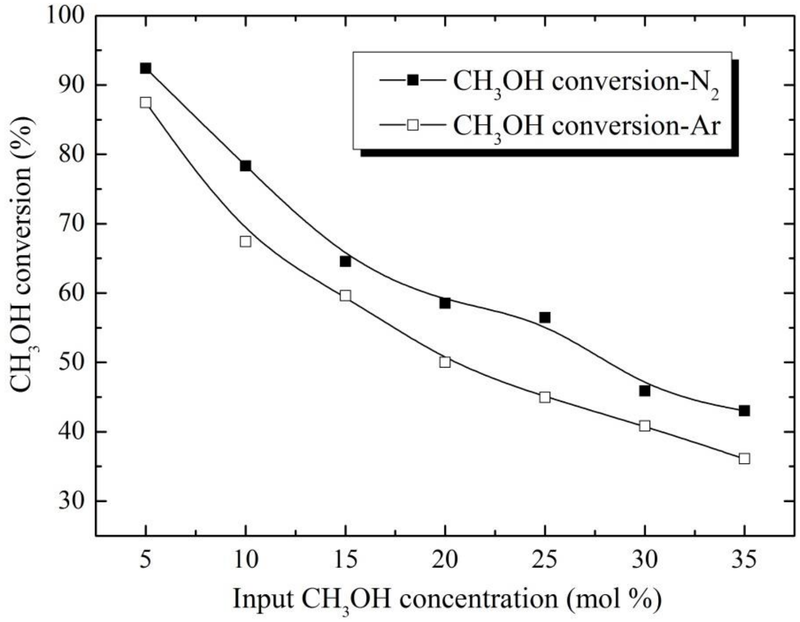

Fig. 3 – Effect of input CH_3OH concentration on CH_3OH conversion

Fig. 4 shows the influence of the CH_3OH concentration on the selectivity of H_2 and CO and the

H_2/CO molar ratio. The selectivity of H_2 and CO produced in the CH_3OH/N_2 RGA is significantly higher than that in the CH_3OH/Ar plasma, especially at a high methanol concentration (> 20%). The effect of the CH_3OH concentration on the selectivity of H_2 and CO shows a similar evolution in both plasma chemical processes: the selectivity of syngas increases almost linearly as the CH_3OH concentration initially increases from 5 to 15 %, and then plateaus to an almost constant value when further increasing the methanol concentration.

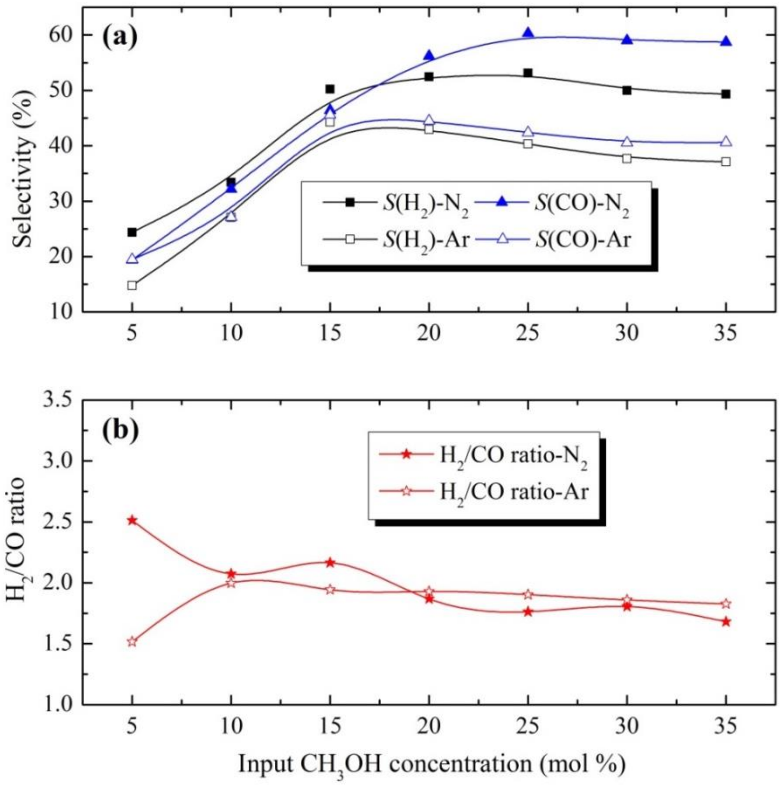

Fig. 4 – Effect of input CH_3OH concentration on (a) H_2 selectivity and CO selectivity; and (b) H_2/CO molar ratio

It is expected that N-containing products (e.g., NH_3 and HCN) were produced in the plasma methanol decomposition process in the CH_3OH/N_2 plasma, as evidenced from the present of NH and CN bands in the emission spectra of the CH_3OH/N_2 plasma.

From the stoichiometry of methanol decomposition reaction, a H_2/CO molar ratio of 2 would be expected. In this study, the H_2/CO ratio is slightly below 2 for most operating conditions. We can see that increasing the CH_3OH concentration from 5 to 10% leads to a noticeable drop of the H_2/CO ratio from 2.51 to 2.07 in the CH_3OH/N_2 plasma, while the H_2/CO molar ratio in the CH_3OH/Ar RGA increases from 1.52 to 2.00. This might be attributed to the formation of different byproducts in both plasma systems. As the methanol concentration increases from 10% to 35%, the H_2/CO molar ratio in the CH_3OH/N_2 plasma slightly decreases, whilst this parameter in the CH_3OH/Ar plasma is almost constant.

Fig. 5 shows the effect of CH_3OH concentration on the selectivities of gaseous byproducts. The selectivity of the gas products (CO_2, CH_4, C_2H_2, and C_2H_4) in the CH_3OH/N_2 plasma decreases in the order: $CH_4 > C_2H_2 > C_2H_4 \approx CO_2$, whilst in the CH_3OH/Ar gliding arc, the selectivity of these gases follows the order $CO_2 > CH_4 > C_2H_2 > C_2H_4$. CO_2 was formed with significantly higher selectivity in the CH_3OH/Ar RGA compared to the CH_3OH/N_2 plasma. Increasing the concentration of CH_3OH from 5 to 35% significantly decreases the CO_2 selectivity from 46.30 to 1.15% in the CH_3OH/Ar plasma. In contrast, the selectivity of CO_2 is almost independent on the input concentration of CH_3OH in the CH_3OH/N_2 plasma and remains low (0.2%).

In the plasma methanol conversion process, CO_2 is more likely to be formed from the reaction of CO with OH radicals (Eq. (8)) [7].

$$CO + OH \rightarrow CO_2 + H \tag{8}$$

Strong OH bands were observed in the spectra of the CH_3OH/Ar plasma, whereas no OH bands were detected in the spectra of the CH_3OH/N_2 RGA (see Fig. 9 and Fig. 10), which suggests that more CO_2 could be produced via Eq. (8) when Ar is used as a carrier gas, leading to a higher CO_2 selectivity. In addition, CO_2 could also be formed from the Boudouard reaction of CO:

$$2CO \rightarrow CO_2 + C \tag{9}$$

Very low selectivity of CO_2 (0.2%) was obtained in the CH_3OH/N_2 RGA, which reveals that this reaction (Eq. (9)) might be inhibited in the plasma methanol conversion process using N_2 as a carrier gas.

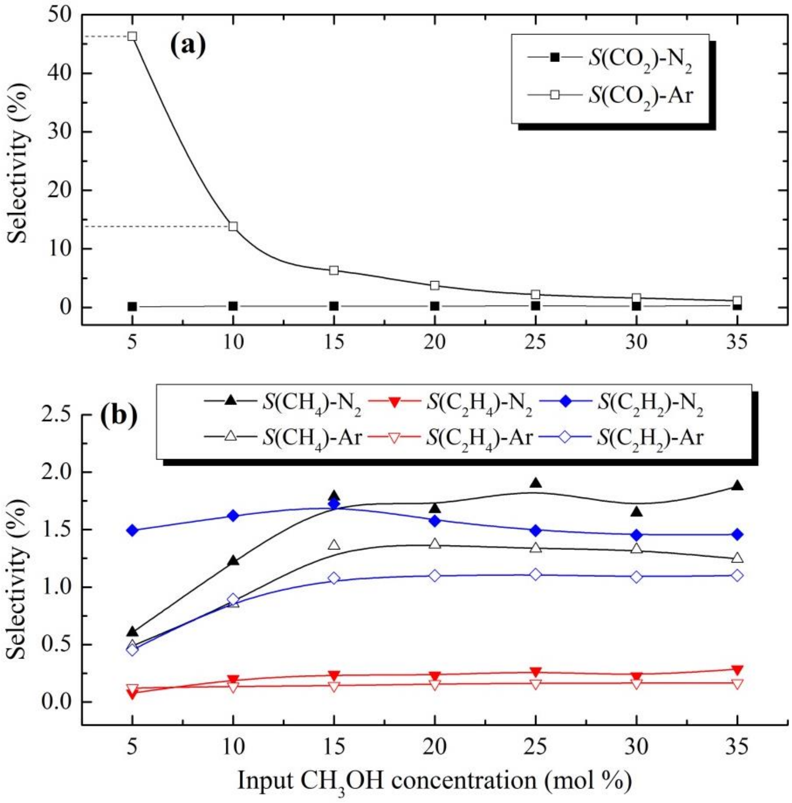

Fig. 5 – Effect of input CH_3OH concentration on the selectivity of gaseous byproducts (a) CO_2, (b) CH_4, C_2H_2, and C_2H_4

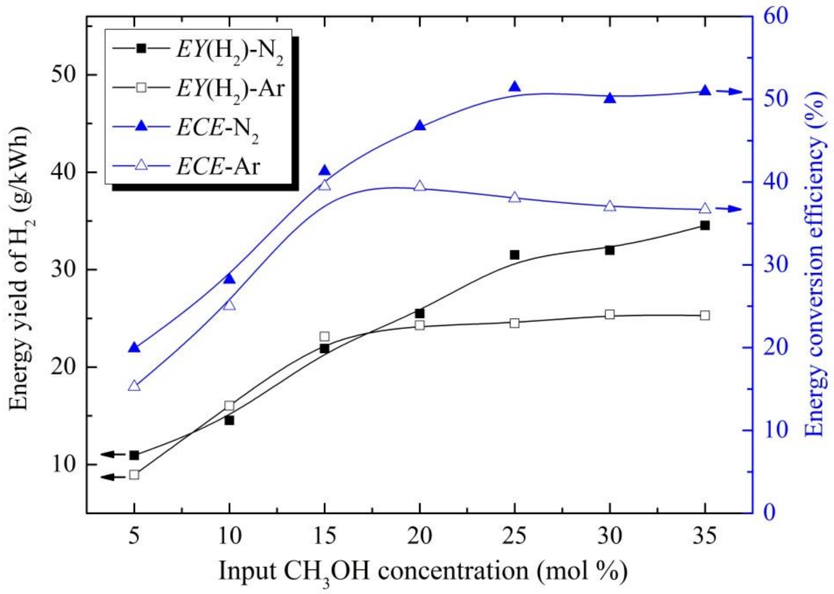

Fig. 6 – Effect of input CH_3OH concentration on energy conversion efficiency and energy yield of H_2

The effect of CH_3OH concentration on the energy conversion efficiency and energy yield of H_2 is presented in Fig. 6. Both parameters follow the similar evolution of the selectivity of H_2 and CO with the increase of the CH_3OH concentration (Fig. 4). At a CH_3OH concentration of higher than 20%, both the energy conversion efficiency and energy yield of H_2 are higher in the CH_3OH/N_2 RGA than those in the CH_3OH/Ar RGA.

We find that the selectivities of gas products are almost constant as the methanol concentration varies between 15% and 35%, except the CO_2 selectivity in the argon plasma process, as shown in Figs. 4 and 5. This phenomenon suggests that there might be no significant changes of the dominant reaction routes in the plasma methanol conversion process. Fig. 7 shows the production of gaseous products increases linearly with increasing the converted methanol at the CH_3OH concentration of 15-35% in the CH_3OH/N_2 plasma. Similar evolution behavior of the gas products (except CO_2) can be found in the Ar plasma-assisted methanol conversion process (Fig. 8). Note that the CO_2 formation decreases linearly with increasing the methanol converted, indicating that there is a significant change in the formation of CO_2. Both reactions can be globally represented by

CH_3OH/N_2 RGA plasma

1 $CH_3OH \rightarrow 0.9993\ H_2 + 0.5801\ CO + 0.0026\ CO_2 + 0.0182\ CH_4 + 0.0073\ C_2H_2 + 0.0013\ C_2H_4 + \ldots$ (10)

CH_3OH/N_2 RGA plasma

1 $CH_3OH \rightarrow 0.7648\ H_2 + 0.4113\ CO + (\text{variable})\ CO_2 + 0.0130\ CH_4 + 0.0055\ C_2H_2 + 0.0008\ C_2H_4 + \ldots$ (11)

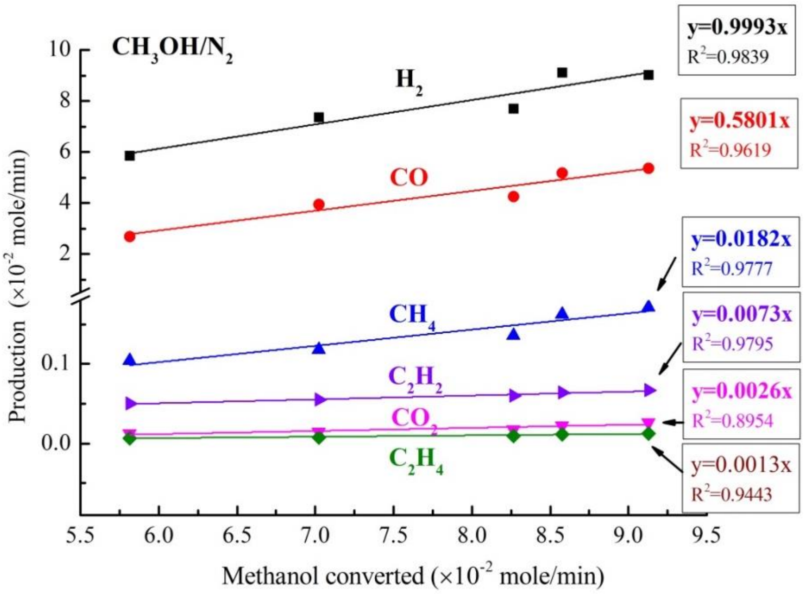

Fig. 7 – Production of gaseous products as a function of methanol converted in the CH_3OH/N_2 RGA at the CH_3OH concentration of 15-35%

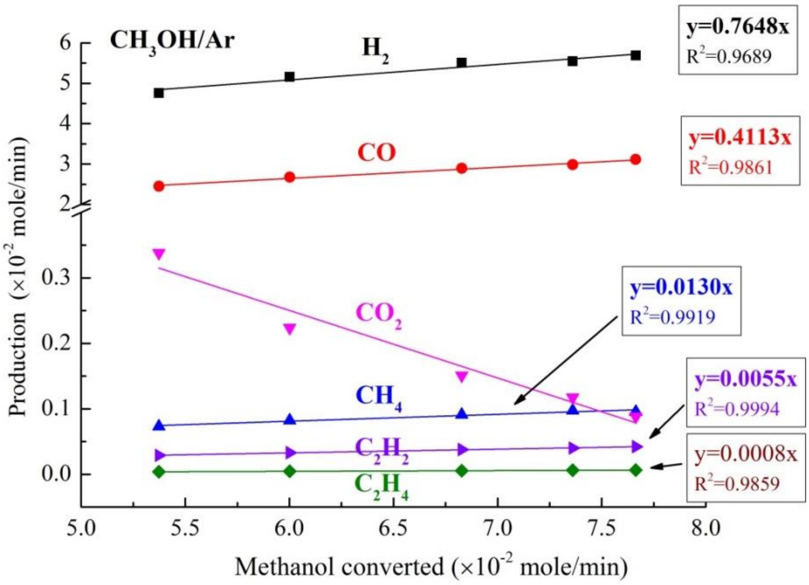

Fig. 8 – Production of gaseous products as a function of methanol converted in the CH_3OH/Ar RGA at the CH_3OH concentration of 15-35%

3.2 Optical diagnostics of plasma chemical processes

Optical emission diagnostics has been carried out to understand the formation of reactive species and to give new insights into the possible reaction mechanisms in the plasma methanol conversion processes. Fig. 9 shows typical emission spectra of the CH_3OH/N_2 RGA. The spectra are clearly dominated by numerous strong CN ($B^2\Sigma \rightarrow X^2\Sigma$, Δv = 1, 0, -1) violet bands at an exposure time of 500 μs. In addition, C I line (193.09 nm), N_2 second positive system ($C^3\Pi_u \rightarrow B^3\Pi_g$), NH ($A^3\Pi \rightarrow X^3\Sigma$) at 336.0 nm, C_2 swan system ($d^3\Pi_g \rightarrow a^3\Pi_u$, Δv =1, 0), and CN violet system of Δv = -2 can be observed using a long exposure time of 25 ms, as plotted in Fig. 9.

Different emission spectra were detected in the CH_3OH/Ar plasma (Fig. 10) to those in the CH_3OH/N_2 RGA. Besides the CN bands due to gas impurity, numerous C_2 swan bands (Δv = 1, 0, -1) and weak CO fourth positive system ($A^1\Pi \rightarrow X^1\Sigma$, Δv = 6-10) can be observed. In addition, OH ($A^2\Sigma^+ \rightarrow X^2\Pi$, Δv = 0) and CH ($A^2\Delta \rightarrow X^2\Pi$, Δv = 0) bands, as well as H Balmer lines (H_α, H_β, and H_δ) can be clearly seen in the spectra. In contrast, these bands (OH, CH, and C_2) and H atomic lines cannot be found in the spectra of the CH_3OH/N_2 RGA. C I spectral lines at 193.09 nm and

247.87 nm, together with numerous argon atomic lines are also visible in the CH_3OH/Ar plasma. Fe spectra lines from the electrode materials are detected in both plasma systems. An overview of these atomic lines and molecular bands that detected in the CH_3OH/N_2 and CH_3OH/Ar plasmas is presented in Table 1.

Vibrational temperature represents the chemical reactivity of vibrational excited species, and provides insight into the relative rates of vibration-vibration and vibration-translation energy exchange processes [28]. The vibrational temperature of CN in the CH_3OH/N_2 RGA was determined from a group of CN ($B^2\Sigma \rightarrow X^2\Sigma$, Δv=0) violet bands using a Boltzmann plot [29]. The results show that increasing the input concentration of CH_3OH from 5 to 35% results in a quasi-linear drop of the vibrational temperature from 14300 ± 800 K to 8930 ± 1300 K in the CH_3OH/N_2 plasma, since CH_3OH could quench the vibrational levels of CN [30]. It is interesting to note that the vibrational temperature in the CH_3OH/N_2 plasma is considerably higher than that of other typical non-thermal plasmas, such as DBD in N_2 or Ar (2000-5000 K) [31-34] and glow discharge in N_2 (2000-4000 K) [35]. In addition, the vibrational temperature in the CH_3OH/N_2 RGA plasma is also found higher than that of a pure N_2 RGA plasma (4000 K) [36] and an air/water gliding arc with knife-shaped electrodes (3900-4500 K) [37], showing higher vibrational levels of

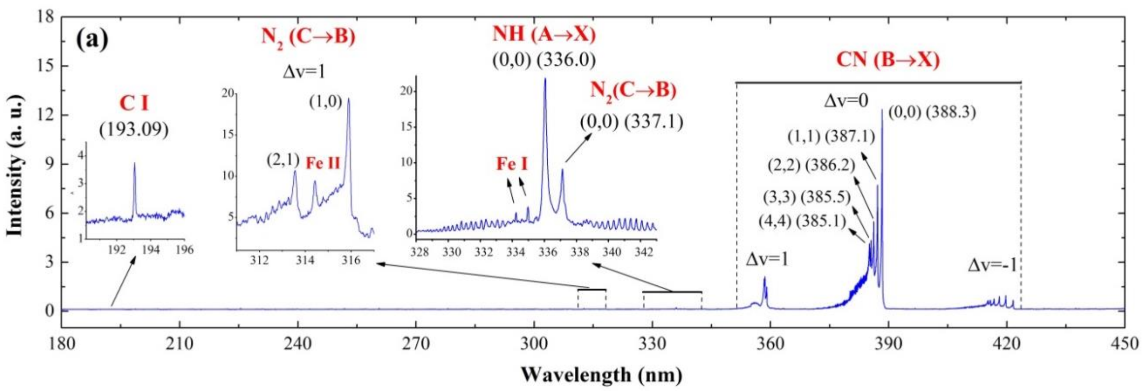

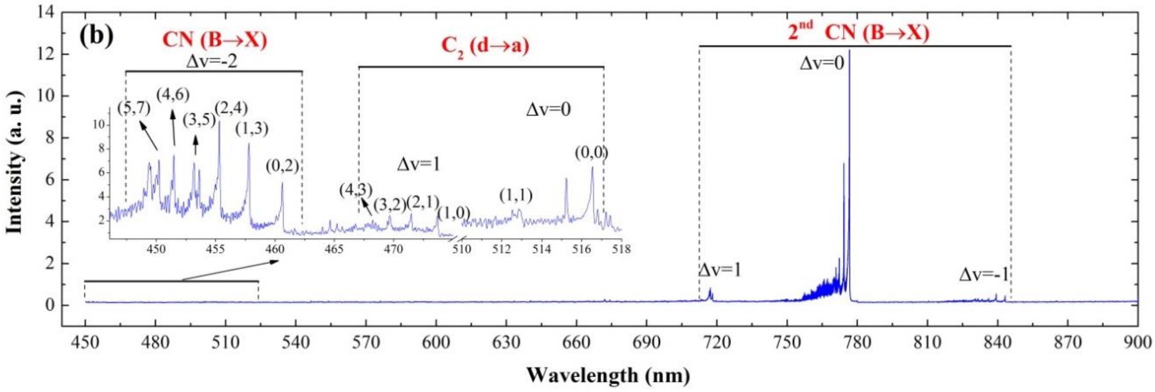

Fig. 9 – Typical emission spectra of the CH_3OH/N_2 plasma (CH_3OH concentration= 5%, exposure time= 500 µs; for enlarged area: exposure time= 25 ms)

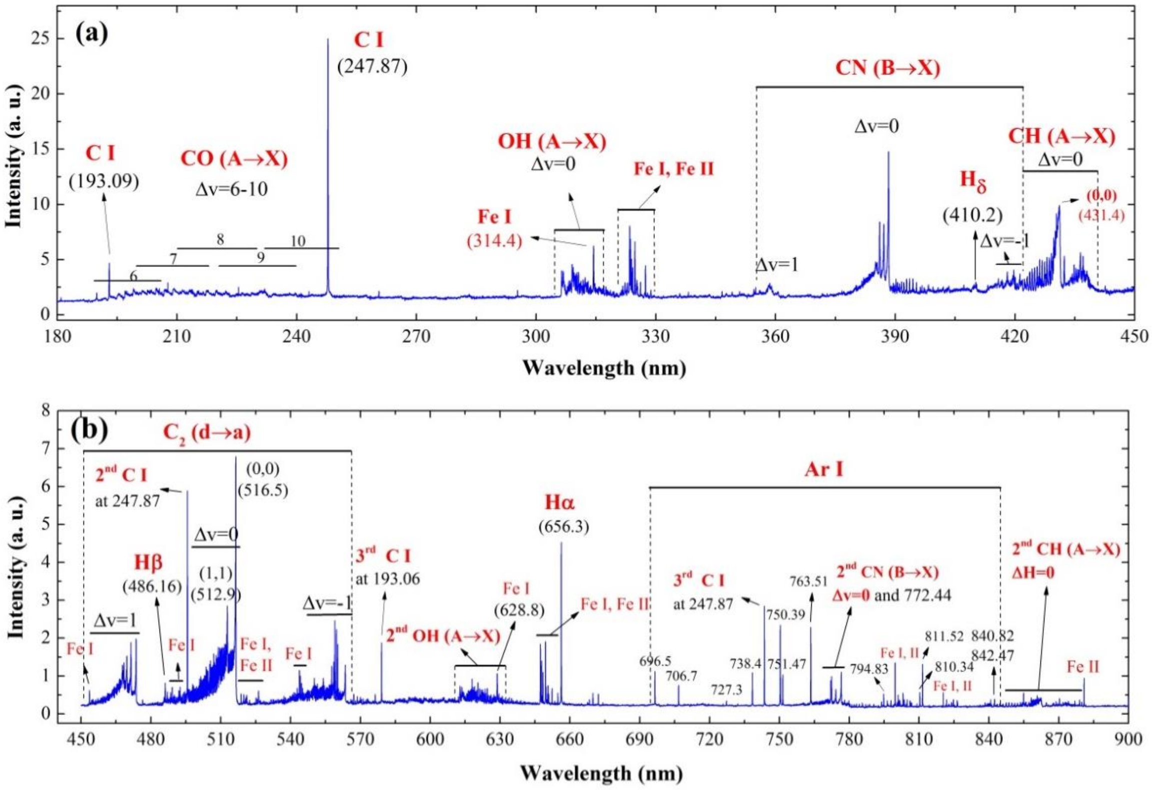

Fig. 10 – Typical emission spectra of the CH_3OH/Ar plasma (CH_3OH concentration= 5%, exposure time= 25 ms)

Table 1 – Overview of the atomic lines and molecular bands in the spectra of the CH_3OH/N_2 and CH_3OH/Ar plasmas

Species	**Transition**	**Wavelength (nm)**	
		CH_3OH/N_2	**CH_3OH/Ar**
C I	$2s^22p^2 \rightarrow 2s^22p3s$	193.09	193.09, 247.87

N_2	$C^3\Pi_u \to B^3\Pi_g$ (2, 1), (1, 0), (0, 0)		312-316, 337.1	ND[a]
NH	$A^3\Pi \to X^3\Sigma$, (0, 0)		336.0	ND
CN	$B^2\Sigma \to X^2\Sigma$	Δv =1, 0, -1	355-360, 376-389, 410-420 2nd order: 715-718.5, 756-777, 808-844	355-360, 376-389, 410-420
		Δv =-2	444-461	ND
C_2	$d^3\Pi_g \to a^3\Pi_u$	Δv = 1, 0	464-474, 512-517	464-474, 512-517
		Δv = -1	ND	546-564
CO	$\mathrm{A}^1\Pi \to \mathrm{X}^1\Sigma$, $\Delta v = 6-10$		ND	190-250
OH	$A^2\Sigma^+ \to X^2\Pi$, $\Delta v = 0$		ND	306-320, 2nd order: 611-640
H	Balmer system	δ	ND	410.2
		β	ND	486.16
		α	ND	656.3
CH	$A^2\Delta \to X^2\Pi$, $\Delta v = 0$		ND	421-440 2nd order:835-880
Ar	-		ND	695-844
Fe	-		314.43, 334.23, 334.98	314.4, 628.8, 647-655, 795-810, 820-827, 880.9

[a] ND: Not detected

the RGA CH_3OH/N_2 plasma. The vibrational temperature of CN in the CH_3OH/Ar plasma was also obtained using the aforementioned method by adding 5 mol % N_2 into the CH_3OH/Ar plasma, and the corresponding vibrational temperature is in the range of 6600 ± 900 to 8100 ± 400 K, which is also much lower than that in the CH_3OH/N_2 plasma.

The electron density of the CH_3OH/Ar plasma can be determined from the Stark broadening of the Ar atomic line at 696.5 nm. The detailed method can be found in previous works [38, 39]. The estimated electron density of the 5% CH_3OH/Ar RGA is $(1.53 \pm 0.14)\times10^{16}$ cm^{-3}. This value is about an order of magnitude lower than that of the AC gliding arc with knife-shaped electrodes [11].

In this study, the electron density obtained in the CH_3OH/Ar and CH_3OH/N_2 RGA plasmas is significantly higher (several orders of magnitude) than that of typical non-thermal plasmas, such as DBD (10^{10}-10^{13} cm^{-3}) and corona discharge (10^{9}-10^{13} cm^{-3}) [11, 40].

3.3 Reaction Mechanisms

The possible dominant reaction pathways in the RGA decomposition of methanol are schematically shown in Fig. 11. At a high concentration of CH_3OH (e.g., 20-35%), electron impact dissociation of methanol via different reaction channels (Eq. (12)-(18)) plays a dominant role in the decomposition of CH_3OH into a variety of radicals or intermediates [41-43], with subsequent radical recombination reactions to form higher hydrocarbons or further dissociation of radicals and intermediates [25].

$$CH_3OH + e \rightarrow CH_3 + OH + e \quad (12)$$

$$CH_3OH + e \rightarrow CH_2OH + H + e \quad (13)$$

$$CH_3OH + e \rightarrow CH_3O + H + e \quad (14)$$

$$CH_3OH + e \rightarrow CH_2 + H_2O + e \quad (15)$$

$$CH_3OH + e \rightarrow \textit{tran}\text{-}HCOH + H_2 + e \quad (16)$$

$$CH_3OH + e \rightarrow \textit{cis}\text{-}HCOH + H_2 + e \quad (17)$$

$$CH_3OH + e \rightarrow CH_2O + H_2 + e \quad (18)$$

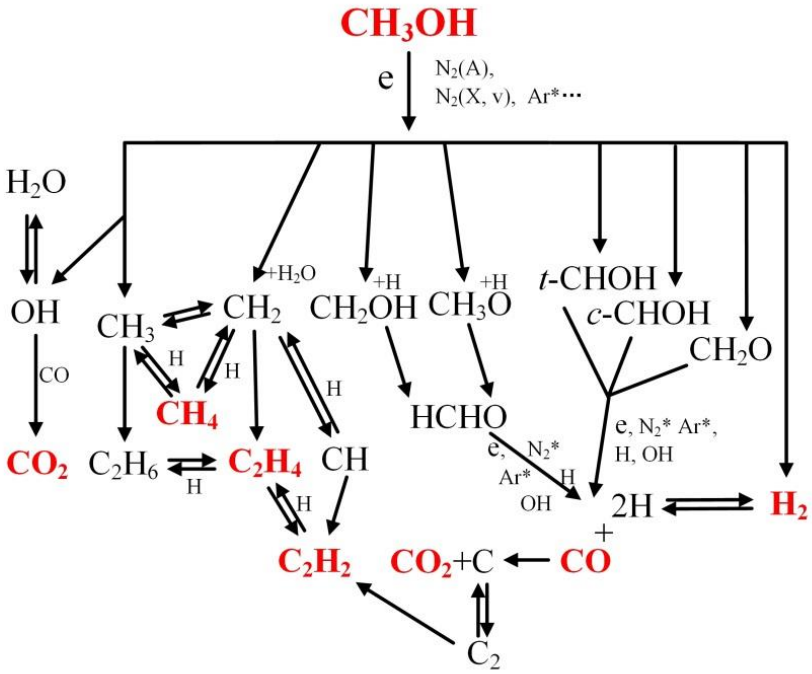

Fig. 11 – Possible reaction pathways of methanol decomposition in CH_3OH/N_2 and CH_3OH/Ar gliding arc plasmas

In the CH_3OH/N_2 and CH_3OH/Ar gliding arc plasmas, initially formed highly energetic electrons interact with the carrier gas (N_2 or Ar) to produce a cascade of processes yielding a variety of chemically reactive species including electronically excited metastable $N_2(A^3\Sigma_u^+)$, vibrationally excited $N_2(X^2\Sigma_g^+, \nu)$, and electronically excited Ar^* species [44-47]. These excited species are believed to make a significant contribution to the dissociation of methanol (Eq. (19)-(21)) into a variety of radicals and intermediates (e.g., CH_3, OH, CH_2O, CH_2OH), especially at a low concentration of methanol (e.g., 5%) [44, 45].

$$CH_3OH + N_2(A^3\Sigma_u^+) \rightarrow \text{radicals and intermediates} + N_2 \quad (19)$$

$$CH_3OH + N_2(X^2\Sigma_g^+, \nu) \rightarrow \text{radicals and intermediates} + N_2(X^2\Sigma_g^+, \nu') \quad (20)$$

$$CH_3OH + Ar^* \rightarrow \text{radicals and intermediates} + Ar \quad (21)$$

Previous plasma modeling work has demonstrated that quenching reactions with metastable nitrogen $N_2(A^3\Sigma_u^+)$ appear to be important in the destruction of ethylene (10-10000 ppm) besides the reactions with radicals in an atmospheric pressure air DBD, while the direct electron impact dissociation reactions are negligible for the destruction of ethylene [47]. Diamy et al. have also shown that metastable N_2 species are critical in the initial decomposition of methane in a CH_4/N_2 glow discharge [30, 48]. In addition, Pintassilgo et al. have demonstrated that the vibrational excited N_2 could contribute much to the decomposition of CH_4 in a 2% CH_4/N_2 afterglow plasma [44, 45]. We can find that more reaction channels for the conversion of methanol exist in the CH_3OH/N_2 plasma due to the formation of more excited species compared to the CH_3OH/Ar plasma, which can also explain the higher conversion of methanol obtained in the plasma reaction using N_2 as a carrier gas.

CH_2O is a key intermediate from the initial decomposition of methanol (Eq. (16)-(21)). CH_2O is unstable in non-thermal plasmas and can be further decomposed to form H_2 and CO through the dissociation with electrons and excited species (e.g., $N_2(A^3\Sigma_u^+)$, $N_2(X^2\Sigma_g^+, v)$, Ar^*),

$$CH_2O + e, N_2(A), N_2(X, v) \rightarrow CHO + H + e, N_2, N_2(X, v') \quad (22)$$

$$CHO + e, N_2(A), N_2(X, v) \rightarrow CO + H + e, N_2, N_2(X, v') \quad (23)$$

$$H + H \rightarrow H_2 \quad (24)$$

H_2 can also be generated from the direct dissociation of methanol (e.g., Eq. 16-21) or the recombination of H radicals from methanol decomposition (e.g., Eq. (24)).

In addition, the H and OH radicals that present in the plasma bulk may also contribute to the conversion of CH_2O and CHO through the following reactions, generating CO, H_2, and H_2O [49].

$$CH_2O + H \rightarrow CHO + H_2 \quad (25)$$

$$CH_2O + OH \rightarrow CHO + H_2O \quad (26)$$

$$CHO + H \rightarrow H_2 + CO \quad (27)$$

$$CHO + OH \rightarrow CO + H_2O \quad (28)$$

Very low selectivities of hydrocarbons (mainly CH_4, C_2H_2 and C_2H_4) have been obtained in the

CH_3OH/N_2 (2.7-3.8%) and CH_3OH/Ar (1.1-2.6%) plasmas. The initially generated CH_3 and CH_2 radicals are the key species to form these hydrocarbons (CH_4, C_2H_2, and C_2H_4) through further dissociation or recombination reactions. For instance, CH_4 can be formed from the recombination of CH_3 and H, which can explain why the selectivity of CH_4 is one order of magnitude higher than that of C_2 hydrocarbons.

Carbon can be mainly formed from the Boudouard reaction (Eq. (9)), which also leads to the formation of CO_2. CO_2 might also be formed via water gas shift reaction (Eq. (29)).

$$CO + H_2O \rightarrow CO_2 + H_2 \tag{29}$$

3.4 Comparison of different plasma technologies for hydrogen production from methanol

Table 2 shows a comparison of the performance (e.g., methanol conversion rate, selectivity of syngas, and energy yield of H_2) of plasma methanol conversion using different processes and plasma systems.

In the steam reforming of methanol using a pulsed gliding arc reactor, a high energy yield of H_2 was achieved with a relatively low conversion of methanol [3]. Note the energy cost for the production of steam has not been considered in the calculation of energy yield of H_2. The combination of plasma with catalysts (e.g., Cu/Al_2O_3 and Cu/ZnO) was also used to enhance the conversion of CH_3OH in the steam reforming of methanol by a DBD [13, 24]. However, the energy efficiency of the plasma-catalytic process is much lower in a DBD plasma reactor compared to that using a gliding arc.

Table 2 – Comparison of the performance of RGA plasmas with other non-thermal plasmas for hydrogen production from methanol conversion

Plasma type	Process	Carrier gas	Reactants	Power supply/ Discharge power	CH_3OH conversion (%)	*S*(H_2) (%)	*S*(CO) (%)	H_2/ CO	*EY*(H_2)[c] (g/kWh)	Ref.
Pulsed GAD	SR[a]	Ar 2 l/min	H_2O + 5-85% CH_3OH: 2-20 ml/min	AC, 250 Hz, 25 kV, 0.3-0.45W	3-33	-	-	-	~50-176	[3]
DBD + Cu/Al_2O catalyst	SR	Ar 10 ml/min	H_2O+50 % CH_3OH; CH_3OH: 0.0165 ml/min	AC, 18.5 kHz ~12.5-21.5 W	15-80	~16-45	-	-	~0.5-16	[13]
DBD + Cu/ZnO catalyst	SR	N_2	H_2O + 50 % CH_3OH; CH_3OH: 0.008 ml/min	AC, 50 kHz, 0-4 kV, 0.12-0.47 W	6-54.4	-	~3-14	-	-	[24]
MHCD	DEC[b]	N_2 10.5-23.7 ml/min	4.7-56.7% CH_3OH	DC, ~0.8-1.3 W	7.4-47.0	55-80	50-80	1.5-2.8	1.2-10.8	[2]
GAD	DEC	Ar 43.3-86.6 ml/min	17.4-37.8% CH_3OH	AC, < 300W	51.8-62.2	43.4-49.5	81.4-81.9	1.14-1.2	~6.9	[4]
Corona	DEC	Ar 40 ml/min	20-75% CH_3OH	AC, 2 kHz 0.8 kV, 12 W	10-80	-	-	-	~4.5	[22]
DBD	DEC	N_2 100 ml/min	1% CH_3OH	AC, 50 Hz, 0.21-1.99 W	8-26	12-21.7	11.7-20.0	1.96-2.70	~0.05-0.63	[15]
RGA	DEC	Ar 7.9-11.5 l/min	5-35% CH_3OH	DC, 10 kV, 105.2-271.6 W	36.1-87.5	14.8-44.3	19.5-45.6	1.52-2.00	8.95-25.40	This work
		N_2 8.8-12.8 l/min		DC, 10 kV, 149.8-349.4 W	43.0-92.4	24.4-53.1	19.4-60.3	1.76-2.51	10.94-34.54	

[a] SR: Steam reforming of methanol

[b] DEC: Non-oxidative decomposition of methanol

[c] The energy yield of H_2 (1 g/kWh) corresponds to the energy cost of 31.67 kJ/mol H_2

In Table 2, we can see that non-oxidative decomposition of methanol offers relatively higher selectivities of H_2 and CO, as well as higher H_2/CO molar ratio, compared with steam reforming of methanol processes due to limited water gas shift reaction. Compared to other plasma systems (e.g.

DBD), the RGA plasma shows a significantly higher conversion of methanol, a relatively high selectivity of syngas, and a highest energy yield of hydrogen in plasma decomposition of methanol process. It is also interesting to note that the RGA plasmas can provide a feed flow rate, or processing capacity, of several orders of magnitude higher (e.g., 7.9-11.5 l/min) than that using other non-thermal plasma systems (e.g., 10.5-100 ml/min in a DBD reactor), whilst allowing for the conversion of a wider range of reactant concentration, both of which are beneficial to the industrial applications.

4. Conclusions

In this study, non-oxidative decomposition of methanol for hydrogen production has been carried out in the atmospheric pressure DC rotating gliding arc plasma reactor. The effect of carrier gas and input CH_3OH concentration on the reaction performance of the plasma conversion processes has been evaluated. The use of N_2 as a carrier gas in the plasma methanol conversion shows much better performance compared with the CH_3OH/Ar gliding arc in terms of the CH_3OH conversion, syngas selectivity, energy yield of H_2, and energy conversion efficiency of the plasma process. It is found that increasing the input methanol concentration from 5 to 35 % significantly decreases the CH_3OH conversion from 92.4 to 43.0 % in the CH_3OH/N_2 RGA and from 87.5 to 36.1 % in the CH_3OH/Ar RGA. Optical emission diagnostics of the plasma process clearly shows the generation of a variety of reactive species in both plasmas. The estimated electron density of the 5% CH_3OH/Ar plasmas is $(1.53 \pm 0.14) \times 10^{16}$ cm^{-3}, which is significantly higher than that of other typical non-thermal plasmas, such as DBD (10^{10}-10^{13} cm^{-3}) and corona discharges (10^{9}-10^{13} cm^{-3}), indicating a high processing capacity of the RGA plasma. The vibrational and electronically excited species (e.g., N_2

($A^3\Sigma_u^+$), N_2($X^2\Sigma_g^+, \nu$), Ar*) are expected to play an important role in the methanol decomposition process. we find that the RGA plasma can provide a feed flow rate, or processing capacity, of several orders of magnitude higher (e.g.,, 7.9-11.5 l/min) than that using other non-thermal plasma systems (e.g., 10.5-100 ml/min in a DBD reactor), whilst allowing for the conversion of a wider range of reactant concentration, both of which are beneficial to the industrial applications.

Acknowledgement

The support of this work by the Specialized Research Fund for the Doctoral Program of Higher Education of China (20120101110099), the Fundamental Research Funds for the Central Universities (2014FZA4011) and the UK EPSRC Bioenergy Challenge Programme (EP/M013162/1) is gratefully acknowledged. H. Zhang acknowledges the support by Lin Guangzhao & Hu Guozan Graduate Education International Exchange Fund.

References

[1] Chen SH, Chen HL, Lee HM, Chao Y. and Chang MB. Review of plasma catalysis on hydrocarbon reforming for hydrogen production—Interaction, integration, and prospects. Appl Catal B 2008, 85(1): 1-9.

[2] Lindner PJ and Besser RS. Hydrogen production by methanol reforming in a non-thermal atmospheric pressure microplasma reactor. Int J Hydrogen Energy 2012, 37(18): 13338-49.

[3] Burlica R, Shih K, Hnatiuc B, and Locke BR. Hydrogen generation by pulsed gliding arc discharge plasma with sprays of alcohol solutions. Ind Eng Chem Res 2011, 50(15): 9466-70.

[4] LÜ Y, Yan W, Hu S, and WANG B. Hydrogen production by methanol decomposition using gliding arc gas discharge. J Fuel Chem. Technol 2012, 40(6): 698-706.

[5] Henriques J, Bundaleska N, Tatarova E, Dias FM, and Ferreira CM. Microwave plasma torches driven by surface wave applied for hydrogen production. Int J Hydrogen Energy 2011, 36(1): 345-54.

[6] Durka T, Stefanidis GD, Van Gerven T, and Stankiewicz AI. Microwave-activated methanol steam reforming for hydrogen production. Int J Hydrogen Energy 2011, 36(20): 12843-52.

[7] Bundaleska N, Tsyganov D, Saavedra R, Tatarova E, Dias FM, and Ferreira CM. Hydrogen production from methanol reforming in microwave ″tornado″type plasma. Int J Hydrogen Energy 2013, 38(22): 9145-57.

[8] Wang Y, You Y, Tsai C, and Wang L. Production of hydrogen by plasma-reforming of methanol. Int J

Hydrogen Energy 2010, 35(18): 9637-40.

[9] Geissler K, Newson E, Vogel F, Truong T, Hottinger P, and Wokaun A. Autothermal methanol reforming for hydrogen production in fuel cell applications. Phys Chem Chem Phys 2001, 3(3): 289-93.

[10] Sá S, Silva H, Brandão L, Sousa JM, and Mendes A. Catalysts for methanol steam reforming—A review. Appl Catal B 2010, 99(1): 43-57.

[11] Tu X and Whitehead JC. Plasma dry reforming of methane in an atmospheric pressure AC gliding arc discharge: Co-generation of syngas and carbon nanomaterials. Int J Hydrogen Energy 2014, 39(18): 9658-69.

[12] Liu SY, Mei DH, Shen Z, and Tu X. Nonoxidative Conversion of Methane in a Dielectric Barrier Discharge Reactor: Prediction of Reaction Performance Based on Neural Network Model. J Phys Chem C 2014, 118(20): 10686-93.

[13] Ge W, Duan X, Li Y, and Wang B. Plasma−catalyst synergy during methanol steam reforming in dielectric barrier discharge micro-plasma reactors for hydrogen production. Plasma Chem Plasma Process 2015, 35(1): 187-99.

[14] Kalra CS, Cho YI, Gutsol A, Fridman A and Rufael TS. Gliding arc in tornado using a reverse vortex flow. Rev Sci Instrum 2005, 71(2): 25110.

[15] Futamura S and Kabashima H. Effects of reactor type and voltage properties in methanol reforming with nonthermal plasma. IEEE Trans Ind Appl 2004, 40(6): 1459-66.

[16] Bo Z, Yan JH, Li XD, Chi Y, and Cen KF. Plasma assisted dry methane reforming using gliding arc gas discharge: Effect of feed gases proportion. Int J Hydrogen Energy 2008, 33(20): 5545-53.

[17] Fridman A, Nester S, Kennedy LA, Saveliev A, and Mutaf-Yardimci O. Gliding arc gas discharge. Prog Energy Combust Sci 1999, 25(2): 211-31.

[18] Tu X, Gallon HJ, and Whitehead JC. Dynamic behavior of an atmospheric argon gliding arc plasma. IEEE Tran Plasma Sci 2011, 39(11): 2900-1.

[19] Zhang H., Du CM, Wu AJ, Bo Z, Yan, JH, and Li XD. Rotating gliding arc assisted methane decomposition in nitrogen for hydrogen production. Int J Hydrogen Energy 2014, 39(24): 12620-35.

[20] Bromberg L, Cohn DR, Rabinovich A, and Alexeev N. Plasma catalytic reforming of methane. Int J Hydrogen Energy 1999, 24(12): 1131-7.

[21] Indarto A, Choi J, Lee H, and Song HK. Effect of additive gases on methane conversion using gliding arc discharge. Energy 2006, 31(14): 2986-95.

[22] Li H, Zou J, Zhang Y, and Liu C. Novel plasma methanol decomposition to hydrogen using corona discharges. Chem Lett 2004, 33(6): 744-745.

[23] Lee DH and Kim T. Plasma-catalyst hybrid methanol-steam reforming for hydrogen production. Int J Hydrogen Energy 2013, 38(14): 6039-43.

[24] Kim T, Jo S, Song Y, and Lee DH. Synergetic mechanism of methanol−steam reforming reaction in a catalytic reactor with electric discharges. Appl Energ 2014, 113: 1692-9.

[25] Tu X and Whitehead JC. Plasma-catalytic dry reforming of methane in an atmospheric dielectric barrier

discharge: Understanding the synergistic effect at low temperature. Appl Catal B 2012, 125: 439-48.

[26] Gallon HJ, Tu X, and Whitehead JC. Effects of reactor packing materials on H_2 production by CO_2 reforming of CH_4 in a dielectric barrier discharge. Plasma Process Polym 2012, 9(1): 90-7.

[27] Yao S, Zhang X, and Lu B. Influence of plasma reactor structure on methanol oxidation. Aiche J 2005, 51(5): 1558-64.

[28] Biloiu C, Sun X, Harvey Z, and Scime E. Determination of rotational and vibrational temperatures of a nitrogen helicon plasma. Rev Sci. Instrum 2006, 77 (10): 10F117.

[29] Ogungbesan B, Kumar R, Su L, and Sassi M. Experimental validation of local thermal equilibrium in a MW plasma torch for hydrogen production. Int J Hydrogen Energy 2013, 38(35): 15210-8.

[30] Legrand JC, Diamy AM, Hrach R, and Hrachova V. Methane Conversion in the Flowing Afterglow of a Dinitrogen Microwave Plasma: Initiation of the Reaction. Contrib Plasma Phys 1997, 37(6): 521-37.

[31] Stanfield SA, Menart J, DeJoseph C, Kimmel RL, and Hayes JR. Rotational and vibrational temperature distributions for a dielectric barrier discharge in air. Aiaa J 2009, 47(5): 1107-15.

[32] Zhang S, Wang W, Jia L, Liu Z, Yang Y, and Dai L. Rotational, vibrational, and excitation temperatures in bipolar nanosecond-pulsed diffuse dielectric-barrier-discharge plasma at atmospheric pressure. IEEE Tran Plasma Sci 2013, 41(2): 350-4.

[33] Masoud N, Martus K, Figus M, and Becker K. Rotational and vibrational temperature measurements in a high−pressure cylindrical dielectric barrier discharge (C−DBD). Contribution Plasma Phys 2005, 45(1): 32-9.

[34] Tu X, Gallon HJ, and Whitehead JC. Electrical and spectroscopic diagnostics of a single-stage plasma-catalysis system: effect of packing with TiO_2. J Phys D: Appl Phys 2011, 44(48): 482003.

[35] Staack D, Farouk B, Gutsol AF, and Fridman AA. Spectroscopic studies and rotational and vibrational temperature measurements of atmospheric pressure normal glow plasma discharges in air. Plasma Sources Sci Technol, 2006, 15(4): 818.

[36] Wu AJ, Zhang H, Li XD, Lu SY, Du CM, and Yan JH. Determination of Spectroscopic Temperatures and Electron Density in Rotating Gliding Arc Discharge. IEEE Tran Plasma Sci 2015, 43(3): 836-45.

[37] Tu X, Yu L, Yan JH, Cen KF, and Chéron BG. Dynamic and spectroscopic characteristics of atmospheric gliding arc in gas-liquid two-phase flow. Phys Plasmas 2009, 16(11): 113506.

[38] Griem HR. Plasma spectroscopy. New York: McGraw-Hill; 1964.

[39] Tu X, Chéron BG, Yan JH, and Cen KF. Electrical and spectroscopic diagnostic of an atmospheric double arc argon plasma jet. Plasma Sources Sci Technol 2007, 16(4): 803.

[40] Tu X, Verheyde B, Corthals S, Paulussen S, and Sels BF. Effect of packing solid material on characteristics of helium dielectric barrier discharge at atmospheric pressure. Phys Plasmas 2011, 18(8): 80702.

[41] Han Y, Wang J, Cheng D, and Liu C. Density functional theory study of methanol conversion via cold plasmas. Ind Eng Chem Res 2006, 45(10): 3460-7.

[42] Chang A and Lin SH. A theoretical study of the $O(^1D) + CH_4$ reaction I. Chem Phys Lett 2002, 363(1): 175-81.

[43] Krasnoperov LN and Michael JV. High-temperature shock tube studies using multipass absorption: rate constant results for OH + CH_3, OH + CH_2, and the dissociation of CH_3OH. J Phys Chem A 2004, 108(40): 8317-23.

[44] Pintassilgo CD and Loureiro J. Kinetic study of a N_2–CH_4 afterglow plasma for production of N-containing hydrocarbon species of Titan’s atmosphere. Adv Space Res 2010, 46(5): 657-71.

[45] Pintassilgo CD and Loureiro J. Production of hydrocarbons and nitriles using a N_2–CH_4 afterglow plasma for simulation of Titan's atmosphere. Planet Space Sci 2009, 57(13): 1621-30.

[46] Hsieh L, Lee W, Chen C, Chang M, and Chang H. Converting methane by using an RF plasma reactor. Plasma Chem Plasma Process 1998, 18(2): 215-39.

[47] Aerts R, Tu X, De Bie C, Whitehead JC, and Bogaerts, A. An investigation into the dominant reactions for ethylene destruction in non−thermal atmospheric plasmas. Plasma Process Polym 2012, 9(10), 994-1000.

[48] Diamy A, Hrach R, Hrachova V, and Legrand J. Influence of C atom concentration for acetylene production in a CH_4/N_2 afterglow. Vacuum 2001, 61(2): 403-7.

[49] Liu C, Mallinson R, and Lobban L. Nonoxidative methane conversion to acetylene over zeolite in a low temperature plasma. J Catal 1998, 179(1): 326-34.